Phase relations in metabasic rocks: constraints from the results of experiments, phase modelling and ACF analysis

C. J. WEI* & Z. Z. DUAN

MOE Key Laboratory of the Orogenic Belt and Crustal Evolution, School of Earth and Space Sciences, Peking University, Beijing 100871, China

Correspondence: cjwei@pku.edu.cn

Abstract: Phase relations in metabasic rocks are documented from the results of phase modelling, experiments and ACF analysis. A P–T pseudosection for a mid-ocean-ridge basalt (MORB) composition was calculated in the P–T range of 1–32 kbar and 400–1100°C using THERMOCALC 3.45. Phase relations in this pseudosection are mostly consistent with the results from experiments but complicated. ACF analyses suggest that the complicated phase relations can be simplified into 10 invariant assemblages involving orthopyroxene, clinopyroxene, hornblende, glaucophane, actinolite, garnet, chlorite, epidote, lawsonite, kyanite and plagioclase, assuming quartz, $NaAlO_2$ and H_2O/melt being are excess. Phase relation analyses in the P–T projections that are constructed according to Schreinemakers' rules and qualitative P–T pseudosections that are obtained for a MORB composition indicate that 22 subfacies assemblages are recognized for metabasic rocks. A four-fold classification of metamorphism is proposed on the basis of the phase relations for metabasic rocks, including low-, medium-, high- and very-high-P/T types, with apparent geothermal gradients >110°C/kbar, between 110 and 55°C/kbar, between 55 and 28°C/kbar, and <28°C/kbar, respectively. This four-fold classification of metamorphism is better able to match various tectonic settings.

The phase relations in metamorphic rocks can be documented through petrographical, experimental and phase-modelling studies. Petrographical observations together with qualitative phase analyses (e.g. ACF and A′KF diagrams) of Eskola (1915, 1939) led to the division of metamorphic facies, such as greenschist, amphibolite, granulite, blueschist and eclogite facies. For quantitatively constraining the phase relations in metabasic rocks, a great number of experiments were carried out. Early experimental studies (before the 1970s) were carried out in great detail on the two end-member systems: H_2O-absent (dry) and H_2O-oversaturated (excess water) to sort out the dry and wet solidi of basic rocks. A few studies *(*e.g. Green & Ringwood 1967) focused on the stabilities of phases such as garnet and plagioclase in dry systems to delineate the transition from granulite facies to eclogite facies. Later experiments started to pay special attention to the melting under fluid-absent conditions because these conditions were considered to prevail in the lower part of the crust (e.g. Clemens & Vielzeuf 1987). Since the beginning of the 1990s, over 200 sets of experiments on amphibole dehydration reactions have been carried out to determine the locations of fluid-absent solidi of amphibolites, the P–T conditions of amphibole-out, and the amounts and compositions of resultant melts (e.g. Beard & Lofgren 1991; Rapp *et al.* 1991, 2003; Rushmer 1991, 1993; Winther & Newton 1991; Sen & Dunn 1994; Qian

& Hermann 2013; Zhang *et al.* 2013; Hastie *et al.* 2016). These experimental results show that the fluid-absent solidi of amphibolites vary mostly between 800 and 900°C, and amphibole-out occurs chiefly at 1000–1100°C. Several experimental studies were performed under subsolidus conditions. For example, Liu *et al.* (1996) studied a basalt–H_2O system to constrain the stabilities of garnet, plagioclase and amphibole, and to document the phase relations in the transition from amphibolite facies to eclogite facies. Schmidt & Poli (1998) presented experimental data on a mid-ocean-ridge basalt (MORB) that was H_2O-saturated in order to discuss the stabilities of phases under subsolidus conditions and the water content bound in hydrous phases.

Since the beginning of the 1990s, phase relations in metamorphic rocks can be quantitatively calculated (phase modelling) using an internally consistent thermodynamic dataset (Holland & Powell 1990, 1998, 2011) and computer software such as THERMOCALC (Powell & Holland 1988; Powell *et al.* 1998), Theriak/Domino (de Capitani & Brown 1987; de Capitani 1994; de Capitani & Petrakakis 2010) and Perple_X (Connolly 1990, 2005). Using this approach, quantitative phase diagrams involving solid solutions can be calculated, including P–T projections, compatibility diagrams, and P–T, T–X and P–X (where P is pressure, T is temperature and X is composition) pseudosections for specific bulk-rock compositions (e.g. Guiraud *et al.*

1990; Powell & Holland 1990; Will *et al.* 1990*a*, *b*; Xu *et al.* 1994; White *et al.* 2001; Wei & Powell 2003, 2004, 2006). The phase-modelling approach has been successfully applied to solving phase relations, *P–T* conditions and evolution histories of natural metamorphic rocks: for instance, high pressure (HP)– ultrahigh pressure (UHP) eclogite mostly under subsolidus conditions (Will *et al.* 1998; Carson *et al.* 1999; Hacker *et al.* 2003, 2013; Wei *et al.* 2003, 2009, 2010, 2013; Wei & Tian 2015). With improvements in the mixing models for amphibole (Diener *et al.* 2007; Diener & Powell 2012; Green *et al.* 2016), pyroxene (Green *et al.* 2007, 2016) and melt (Green *et al.* 2016), phase equilibria for the melting process in metabasic rocks can be well modelled (Palin *et al.* 2016*b*).

Quantitative phase modelling suggests that the *P–T* pseudosections of most metabasic rocks show similar but very complicated phase relations. Generally, these pseudosections are not easy to read and the phase relations are difficult to understand. Some authors provided associated summary or petrological phase diagrams alongside their calculated pseudosections (e.g. Palin *et al.* 2016*a*). Thus, one aim of this study is to present simplified phase relations from the viewpoint of ACF analysis following the basic notions in Eskola (1915). The other aim of this study is to compare whether the results from a phase-modelling approach are consistent with those from experiments for metabasic rocks. Moreover, on the basis of the simplified phase relations derived from the ACF analysis, a four-fold classification of metamorphism is proposed following the basic notions in Miyashiro (1961, 1994) and Brown (2007).

Phase relations calculated for a MORB composition using THERMOCALC

The *P–T* pseudosection calculated for the MORB compositions of Sun & McDonough (1989) (Table 1) in the *P–T* range of 1–32 kbar and 400–1100°C is shown in Figure 1. The model system NCKFMASHTO (Na$_2$O–CaO–K$_2$O–FeO–MgO–Al$_2$O$_3$–SiO$_2$–H$_2$O–TiO$_2$–Fe$_2$O$_3$) was chosen where P$_2$O$_5$ and MnO are neglected because they are mainly

present in apatite and garnet, and incorporated only in trivial amounts in the other silicate minerals in the *P–T* range of interest. Fluid is considered to be pure H$_2$O and in excess in the subsolidus conditions. In the suprasolidus conditions, the modelled water content was adjusted so that the minimal free fluid (*c.* 1 mol%) was present at the 8 kbar solidus to ensure that the solidus remained fluid-saturated over the entire *P–T* range of interest. The bulk-rock O content was defined by assuming XFe^{3+} = Fe^{3+}/ (Fe^{3+} + Fe^{2+}) = 0.12 (Rebay *et al.* 2010). Pseudosection calculations were performed using THERMOCALC 3.45 (Powell *et al.* 1998), using the February 2012 updated version of the Holland & Powell (2011) dataset (file tc-ds62.txt). The *a–x* relations for the phase are from Green *et al.* (2016).

Two clinopyroxene mixing models were used for the phase modelling, where the augite model (Green *et al.* 2016) was used to calculate the suprasolidus phase relations of low pressure in the sillimanite field, and the omphacite/diopside model (Green *et al.* 2016) was used to calculate the subsolidus and suprasolidus phase relations of high pressure in the kyanite field. Thus, some phase boundary curves are dislocated along the boundary line between kyanite and sillimanite in Figure 1. The omphacite and diopside are defined using the calculated isopleth with jadeite of 0.20 in clinopyroxene. As shown in Figure 1, the fluid-saturated solidus (bold red curve) has negative slopes at pressures below 11 kbar and positive slopes at higher pressures above 11 kbar, occurring at 690°C/5 kbar, 620°C/ 11 kbar and 800°C/25 kbar. The used water content is mostly appropriate as it is consumed immediately above the solidus at pressures of between 4 and 27 kbar, but apparently in excess at pressures below 4 kbar and above 27 kbar.

K$_2$O-bearing phases include biotite and muscovite, the transition between which occurs at 9–13 kbar, with biotite being a low-pressure phase and muscovite being a high-pressure phase. Both of them are mostly stable under subsolidus conditions and tend to disappear above the solidus. Schmidt & Poli (1998) proposed that muscovite in basic rocks may be consumed on the solidus. This may be true only when fluid is oversaturated: for instance,

Table 1. *Chemical compositions of representative basic rocks (MORB) (wt%)*

	SiO$_2$	TiO$_2$	Al$_2$O$_3$	Fe$_2$O$_3$	FeO	MnO	MgO	CaO	Na$_2$O	K$_2$O	P$_2$O$_5$	Mg#	A	C	F
1	49.20	2.03	16.09	2.72	7.77	0.18	6.44	10.46	3.01	0.14	0.23	0.53	21.6	32.0	46.4
2	50.53	1.35	14.88	–	9.39	0.18	8.22	10.99	2.60	0.34	0.13	0.61	18.5	31.9	49.6
3	52.40	1.60	16.90	–	10.30	–	7.10	10.10	3.20	0.10	–	0.55	21.5	30.4	48.1
4	50.64	1.63	15.09	–	10.28	0.19	7.41	11.16	2.89	0.21	0.18	0.56	18.9	32.9	48.3

Mg# = MgO/(MgO + FeO(total)).
1, Engel *et al.* (1965); 2, Sun & McDonough (1989); 3, Schmidt & Poli (1998); 4, Gale *et al.* (2013).

Fig. 1. *P–T* pseudosection for metabasic rocks with a MORB composition (Sun & McDonough 1989) (Table 1) in the system NCKFMASHTO (+ H₂O/L + q/coe). The bulk-rock composition is normalized on the basis of mol% as: $SiO_2 = 50.086$, $Al_2O_3 = 8.691$, $CaO = 11.671$, $MgO = 12.145$, $FeO = 7.784$, $K_2O = 0.215$, $Na_2O = 2.498$, $TiO_2 = 1.006$, $O = 0.467$. *P–T* pseudosection in the suprasolidus conditions is calculated with $H_2O = 5.437$, which is defined according to the method mentioned in the text. '-q' denotes quartz-absent assemblages; 'jd20' denotes the calculated isopleth with jadeite of 0.20 in clinopyroxene. The transition lines of andalusite, kyanite and sillimanite, quartz and coesite, and the reactions jd + q = ab and law = zo + ky + q + H₂O calculated using THERMOCALC are shown in dashed lines. A few of the phase boundary curves are dislocated along the transition line between kyanite and sillimanite because two clinopyroxene mixing models were used (see the text). Abbreviations: ab, albite; act, actinolite; and, andalusite; aug, augite; bi, biotite; chl, chlorite; coe, coesite; di, diopside; ep, epidote; g, garnet; gl, glaucophane; hb, hornblende; ilm, ilmenite; jd, jadeite; ky, kyanite; L, silicate melt; law, lawsonite; mu, muscovite; o, omphacite; opx, orthopyroxene; pl, plagioclase; q, quartz; ru, rutile; sill, sillimanite; sph, sphene; ta, talc.

at *P* > 27 kbar as shown in Figure 1. If fluid is absent, biotite will disappear just above the solidus, but muscovite can survive for more than 100°C above the solidus. TiO₂-bearing phases include rutile, sphene and ilmenite. Three of them coexist at a small domain of *c*.

7.5 kbar/790°C. From this domain, the transition curves between sphene and rutile first show positive slopes at lower-pressure garnet-absent fields, and are changed to moderately negative to flat slopes in the higher pressure fields with both garnet and

hornblende. In the high-P/T fields with glaucophane, the transition curves between sphene and rutile show moderately negative slopes. The transition curves between sphene and ilmenite show moderately positive slopes above the solidus, but become flat below the solidus. The transition curves between rutile and ilmenite show moderate to flat slopes below 1000°C, and become steeply negative in higher temperatures. SiO$_2$ phases include quartz and coesite, which become absent in the assemblages at the

lower right-hand corner (e.g. <4 kbar/500–800°C or <25 kbar/>800°C) and the upper left-hand corner of >15 kbar/<520°C in Figure 1.

Comparison of phase relations constrained between experiments and phase modelling

Figure 2 shows the compilation of experimentally constrained stabilities of major phases in metabasic

Fig. 2. Comparison of the stability limits of phases in metabasic rocks constrained from the phase modelling in Figure 1 (thin dashed curves) and from the experimental data (bold solid curves) with detailed labels. The experimental data are: G67, Green (1967); GR67, Green & Ringwood (1967); LBE96, Liu *et al.* (1996); LW72, Lambert & Wyllie (1972); R91: Rushmer (1991); RW95, Rapp & Watson (1995); SD94, Sen & Dunn (1994); SP98, Schmidt & Poli (1998); WN91, Winther & Newton (1991); WW93, Wyllie & Wolf (1993). FSS, fluid-saturated solidus; FAS, fluid-absent solidus. The division of metamorphic facies was from Brown (2014). The abbreviations of metamorphic facies: AM, amphibolite facies; BS, blueschist facies; E-HPG, eclogite-high pressure granulite facies; GR, granulite facies; GS, greenschist facies. UHP, ultrahigh-pressure eclogite facies. The other abbreviations are the same as shown for Figure 1.

rocks, and a comparison with those from the phase-modelling results in Figure 1 and the division of metamorphic facies from Brown (2014). The stability limits of amphibole (am-out) under suprasolidus conditions controlled by dehydration melting reactions vary diversely in different experiments (Moyen & Stevens 2006). Generally, the am-out curves show positively steep slopes and range from 900 to 1100°C in the garnet-absent assemblages below 10 kbar. Whereas in the garnet-bearing assemblages above 10 kbar, the am-out curves show negative slopes with temperatures ranging from 700 to 1100°C and a maximum pressure condition of <24 kbar (Wyllie & Wolf 1993; Sen & Dunn 1994). Data from Schmidt & Poli (1998) suggest that the upper-pressure limit of amphibole under subsolidus conditions is less than 24 kbar and varies trivially as temperature changes. The calculated upper-temperature limit of amphibole or hornblende (*sensu lato*) under suprasolidus conditions is similar to the experimental results, showing positive slopes in the garnet-absent assemblages below 10 kbar, but negative slopes in the higher-pressure garnet-bearing assemblages with pressures slightly lower than the experimental results (Wyllie & Wolf 1993; Sen & Dunn 1994). Under subsolidus conditions, amphibole includes three categories: hornblende, actinolite and glaucophane (see Diener *et al.* 2007). The lower-temperature limit of hornblende shows positively steep slopes, with temperatures ranging from 420 to 660°C, and pressures from 1 to 23 kbar. Glaucophane is stable under low-temperature (<660°C) and high-pressure (>9 kbar) conditions. Actinolite is stable under low-temperature conditions of <500–600°C, and pressures of <30 kbar. The calculated upper-pressure limits of amphibole are much higher than the experimental results of Schmidt & Poli (1998).

The stability limits of plagioclase (pl-out) are controlled by fluid/melt behaviours and bulk-rock compositions. As suggested from experiments in dry systems, the pl-out limits are 20 kbar/1100°C in dry quartz tholeiites (Green & Ringwood 1967) and 24 kbar/1100°C in high-Al basalts (Green 1967). These pl-out curves show moderately positive slopes, with their pressure decreasing as temperature drops. The pl-out limits constrained by experiments for amphibole dehydration melting (e.g. Rapp & Watson 1995) show negatively steep slopes with temperatures up to 1000–1100°C. The experimental data in Liu *et al.* (1996) suggest that the pl-out curve shows a positive slope under $T < 730$°C conditions but shows negative slopes at $T > 730$°C. The calculated upper-pressure limit of plagioclase shows moderately positive slopes in the temperature range of 600–900°C, similar to the experimental results of Liu *et al.* (1996), but steeply positive slopes in the lower temperatures of <600°C with a coexistence of albite, and negative slopes in the higher temperatures

beyond the stability of hornblende. The calculated upper-pressure limit of albite shows a gently positive slope at 9–11 kbar. The negative slopes for the stability limits of plagioclase in the high-temperature melt-bearing assemblages can be attributed to the fact that the suprasolidus plagioclase tends to be dissolved into the melt, and the stability of plagioclase is reduced as the water content increases (Winther & Newton 1991). The upper-pressure limits of plagioclase may show positive slopes in natural anatectic rocks if melt loss occurs.

The stability limits of garnet (gt-in) are consistent in different experiments for metabasic rocks, which show flat slopes with pressures of 8–10 kbar/600–900°C (e.g. Liu *et al.* 1996; Schmidt & Poli 1998) and their slopes become steeper at temperatures higher than 900°C (e.g. Rapp & Watson 1995). The calculated gt-in curves are slightly lower than the experimental results at temperatures of >900°C, but shows negatively moderate slopes in the temperature range of 500–900°C, and almost vertical slopes at lower temperatures of <500°C.

Compared with the stabilities of lawsonite, zoisite/epidote and chlorite experimentally constrained by Schmidt & Poli (1998) for a H_2O-saturated MORB system, the calculated results are slightly larger for lawsonite, but much smaller for both epidote/zoisite and chlorite. The calculated H_2O-saturated solidus is intermediate between the experimental results of Lambert & Wyllie (1972) and Schmidt & Poli (1998) at pressures of between 4 and 17 kbar, but shows higher temperatures above 17 kbar and lower temperatures below 4 kbar.

ACF analyses of the phase relations in metabasic rocks

ACF plot

The major minerals in most metabasic rocks may include plagioclase, amphibole, garnet, clinopyroxene, orthopyroxene, chlorite, epidote, lawsonite, kyanite, quartz and fluid/melt. The end members of these minerals are presented in Table 2, which can be modelled in the model system NCFMASH (N_2O–CaO–FeO–MgO–Al_2O_3–SiO_2–H_2O). These components are incorporated into three component groups including A (=Al_2O_3–Na_2O), C (=CaO) and F (=FeO + MgO) if assuming SiO_2, H_2O and $NaAlO_2$ components are in excess, and nominated as ACF components herein. The $NaAlO_2$ component may represent albite in plagioclase, jadeite in clinopyroxene, and glaucophane in amphibole. The major minerals in metabasic rocks and their end members are ploted in Figure 3 taking into account the ACF values in Table 2. Garnet is a solid solution including pyrope, almandine and grossular, and plots

Table 2. *Major minerals in metabasic rocks in the NCFMASH system*

Minerals	End members	Chemical formula	A	C	F
Plagioclase (pl)	Anorthite (an)–albite (ab)	$CaAl_2Si_2O_8$–$NaAlSi_3O_8$	1/2	1/2	0
Amphibole (am)	Glaucophane (gl)	$Na_2Mg_3Al_2Si_8O_{22}(OH)_2$	0	0	1
	Tremolite (tr)	$Ca_2Mg_5Si_8O_{22}(OH)_2$	0	2/7	5/7
	Barroisite (bar)	$NaCaMg_4Al_3Si_7O_{22}(OH)_2$	1/6	1/6	4/6
	Winchite (win)	$NaCaMg_4AlSi_8O_{22}(OH)_2$	0	1/5	4/5
	Edenite (ed)	$NaCa_2Mg_5AlSi_7O_{22}(OH)_2$	0	2/7	5/7
	Hornblende (hb)	$Ca_2Mg_4Al_2Si_7O_{22}(OH)_2$	1/7	2/7	4/7
	Pargasite (par)	$NaCa_2Mg_4Al_3Si_6O_{22}(OH)_2$	1/7	2/7	4/7
	Tschermakite (ts)	$Ca_2Mg_3Al_4Si_6O_{22}(OH)_2$	2/7	2/7	3/7
Garnet (gt)	Almandine (alm)–pyrope (py)	$Fe_3Al_2Si_3O_{12}$–$Mg_3Al_2Si_3O_{12}$	1/4	0	3/4
	grossular (gr)	$Ca_3Al_2Si_3O_{12}$	1/4	3/4	0
Clinopyroxene (di/om)	Diopside(di)-hedenbergite (hd)–jadeite(jd)	$CaMgSi_2O_6$–$CaFeSi_2O_6$–$NaAlSi_2O_6$	0	0.5	0.5
Orthopyroxene (opx)	Enstatite (en)–ferrosilite (fs)	$Mg_2Si_2O_6$–Fe_2Si_2O6	0	0	1
Chlorite (chl)	Chlonochlore–amesite	$Mg_5Al_2Si_3O_{10}(OH)_8$	1/6	0	5/6
		$Mg_4Al_4Si_2O_{10}(OH)_8$	2/6	0	4/6
Epidote (ep)	Clinozoisite–epidote	$Ca_2Al_3Si_3O_{12}(OH)$–$Ca_2FeAl_2Si_3O_{12}(OH)$	3/7	4/7	0
Lawsonite (law)		$CaAl_2Si_2O_6(OH)_4$	1/2	1/2	0
Kyanite (ky)		Al_2SiO_5	1	0	0

as a black solid bar if a grossular content of 0–30% is assumed, which will vary according to different *P–T* conditions in the following discussion. Amphibole contains eight end members (Leake *et al.* 1997), and
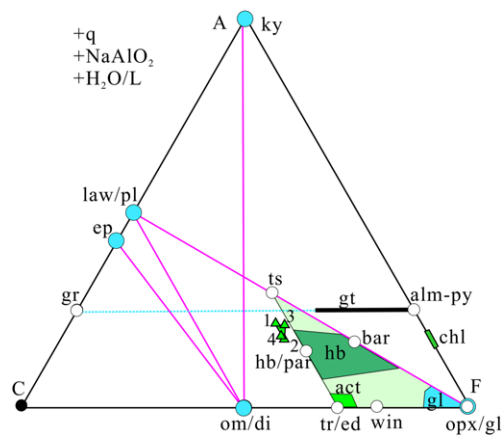
Fig. 3. ACF diagram showing the projection of major minerals (big blue circle) and end members (small white circles) in metabasic rocks. The four MORB compositions are also plotted as small green triangles with labels consistent with those in Table 1. All of the amphibole end members plot in the gl–tr–ts triangle and the three amphiboles, including hornblende (hb), actinolite (act) and glaucophane (gl), qualitatively plot as darker shadowed fields. q, quartz; L, melt. For the other abbreviations see Table 2.

all of them plot in the gl–tr–ts triangle in Figure 3. Following Dale *et al.* (2005) and Diener *et al.* (2007), amphibole is classified into three phases including hornblende (hb) (*sensu lato*), actinolite (act) and glaucophane (gl), which qualitatively plot as darker shadowed fields in Figure 3. Chlorite is qualitatively plotted with varying amounts of tschermak substitution. The other minerals plot with a specific composition. For the phase equilibria under suprasolidus conditions, melt (L) is present as an excess phase.

The other components including K_2O, TiO_2, Fe_2O_3, MnO and P_2O_5, nominated as non-ACF components, are present in trivial amounts in metabasic rocks, and occur as independent phases, such as muscovite, biotite, K-feldspar, rutile, sphene, ilmenite, magnetite and apatite, etc., or substitute the ACF components in silicate minerals. For instance, minor amounts of Fe^{3+} can replace Al, and Mn substitutes Fe^{2+} and Mg in minerals. These non-ACF components may take subordinate roles in controlling the phase relations of metabasic rocks. Figure 3 also shows the projections of the four MORB compositions presented in Table 1. Their A, C and F values were calculated by assuming that all TiO_2 is present in ilmenite, Fe_2O_3 takes up 10% of total FeO and substitutes Al_2O_3, and P_2O_5 is present in apatite.

ACF analysis of phase relations

Taking into account the mineral phases in Figure 3 and combining them with their stabilities constrained

from both experiments and phase modelling, 10 invariant assemblages are involved in illustrating the phase relations of metabasic rocks. Their detailed information is presented in Table 3 and Figure 4. Each invariant assemblage includes five univariant assemblages or reactions, which constrain the division of five metamorphic facies (Fig. 4) and metamorphic subfacies (for details, see below).

The P–T locations of the ACF invariant points and univariant reactions were constrained mostly on the basis of the calculated equilibria in Figure 1 and the experimental data shown in Figure 2. For example, points i1, i2, i4 and i5 are defined according to the calculated low-temperature limits of hornblende together with the high-pressure limits of plagioclase (i1), the low-pressure limits of glaucophane (i2), and the low-formation of garnet (i5) and omphacite (i4). The P–T conditions of points i3 and i9 are constrained on the basis of the calculated low-pressure limits of lawsonite together with the formation of garnet and kyanite. Point i6 is defined on the low-pressure limits of garnet experimentally constrained by Liu et al. (1996) and the fluid-absent solidi of amphibolite (Rushmer 1991; Winther & Newton 1991), which is consistent with the calculated low-temperature limits of orthopyroxene in Figure 1. The P–T conditions for points i7 and i8 are defined by the calculated high-pressure limits of plagioclase and experimentally-defined high-temperature limits of epidote (Schmidt & Poli 1998),

combined with the approximate low-pressure limits of garnet experimentally constrained by Liu et al. (1996). Point i10 is consistent with the experimentally constrained high-pressure limits of plagioclase (Liu et al. 1996) and high-temperature limits of epidote (Schmidt & Poli 1998).

Five metamorphic facies assemblages can be defined in Figure 4. The diagnostic mineral parageneses are chl + act for greenschist facies, hb + pl/ab for amphibolite facies, opx + pl or di + gt + pl for granulite facies, gl + ep/law for blueschist facies and gt + om for eclogite facies. The higher-pressure part of the amphibolite facies includes assemblages deficient in both plagioclase and albite.

Phase relations in the transition between metamorphic facies

Phase relations under greenschist, amphibolite and blueschist facies

The possible minerals present in metabasic rocks under greenschist, amphibolite and blueschist facies may include actinolite, hornblende, glaucophane, chlorite, plagioclase and epidote, if assuming quartz, water and $NaAlO_2$ in excess. These minerals construct two invariant assemblages (i1 and i2) and their ACF plots are shown in Figure 5a, b. The possible univariant reactions are listed in Table 3.

Table 3. *Univariant reactions of approximate* P–T *conditions of 10 invariant assemblages in metabasic rocks*

i1, pl + ep + hb + act + chl	i2, gl + ep + hb + act + chl	i3, law + om + gl + gt + ep	i4, gl + ep + hb + gt + om	i5, gl + ep + hb + gt + chl
3kbar/470°C	9.5 kbar/490°C	18 kbar/505°C	15 kbar/590°C	13.5 kbar/510°C
(pl) chl + act + ep = hb	(gl) ep + chl + act = hb	(law) gl + ep = gt + om	(gl) hb + ep = gt + om	(gl) chl + ep = gt + hb
(ep) pl + act + chl = hb	(ep) act + chl = hb + gl	(om) gl + law = gt + ep	(ep) gt + om + gl = hb	(ep) gl + gt = hb + chl
(hb) ep + chl = pl + act	(hb) ep + gl = act + chl	(gl) om + law = gt + ep	(hb) gl + ep = gt + om	(hb) gl + gt = ep + chl
(act) ep + chl = pl + hb	(chl) ep + gl + act = hb	(gt) law + om = gl + ep	(gt) gl + om + ep = hb	(gt) ep + gl = hb + chl
(chl) pl + act = ep + hb	(act) ep + gl = hb + chl	(ep) law + gl = gt + om	(om) gl + ep = gt + hb	(chl) gl + ep = gt + hb
i6, pl + hb + di + opx + gt	i7, pl + ep + hb + di + gt	i8, pl + ep + hb + gt + chl	i9, law + ep + gt + om + ky	i10, pl + ep + gt + om + ky
10 kbar/810°C	10 kbar/700°C	9 kbar/590°C	25 kbar/640°C	14 kbar/710°C
(pl) hb = gt + di + opx	(pl) ep + hb = gt + di	(pl) chl + ep = gt + hb	(law) gt + ep = om + ky	(pl) gt + ep = om + ky
(hb) opx + pl = di + gt	(ep) pl + hb = gt + di	(ep) pl + chl = gt + hb	(ep) gt + law = om + ky	(ep) gt + pl = om + ky
(di) hb + gt = pl + opx	(hb) gt + ep = di + pl	(hb) pl + chl = gt + ep	(gt) law = ep + ky	(gt) pl = ep + ky
(opx) pl + hb = gt + di	(di) ep + gt = pl + hb	(gt) ep + chl = pl + hb	(om) law = ep + ky	(om) pl = ep + ky
(gt) hb = opx + di + pl	(gt) ep + hb = di + pl	(chl) pl + hb = gt + ep	(ky) law + om = gt + ep	(ky) gt + ep = di + pl

Fig. 4. *P–T* diagram showing the stabilities of 10 ACF invariant assemblages with numbers corresponding to those in Table 3; univariant reactions are labelled with the absent phase and the extent of five metamorphic facies. The stability limits of minerals and fluid-saturated solidi from experiments and phase modelling are the same as those in Figure 2. The abbreviations: EC, eclogite facies. The other abbreviations are the same as shown for Figures 1 and 2.

According to Schreinemakers' rules (e.g. Zen 1966), the topological relationships between these reactions are shown in Figure 5c. It also shows the diagnostic (shaded) and non-diagnostic assemblages in each divariant field bounded by the univariant reactions, which is the *P–T* projection that shows phase relations for all bulk-rock compositions in the ACF space (Powell *et al.* 1998). For a specific composition, only one assemblage is stable in each divariant field, which is called the *P–T* pseudosection. For the MORB composition of interest (M in Fig. 5a, b), its *P–T* pseudosection can be qualitatively analysed, as shown in Figure 5d. Only one reaction i2-(ep) (refers to the epidote-absent reaction around point i2) cannot be seen by the composition. According to Figure 5d, six metamorphic subfacies can be classified. The diagnostic assemblage of albite greenschist subfacies (ab-GS) is act + ep + chl (+ab + q). A progressive change with *P–T* conditions below invariant point i1 is characteristic of the

appearance of act + pl via reaction i1-(hb), producing a subfacies assemblage named as the plagioclase greenschist subfacies (pl-GS), which is followed by the appearance of hornblende via reaction i1-(ep), and the disappearance of actinolite via reaction i1-(chl), resulting in the formation of two subfacies assemblages: the actinolite-bearing low-temperature amphibolite (act-LAM) and low-temperature amphibolite (LAM). However, a progressive change with *P–T* conditions above invariant point i1 is marked by the appearance of hornblende via the reaction i1-(pl) or i2-(gl), forming an assemblage (hb + ep + chl + ab + q) of epidote amphibolite subfacies (ep-AM). The ep-AM assemblage is transformed into the LAM subfacies via reaction i1-(act), marked by the formation of plagioclase and disappearance of albite. The transition from greenschist to blueschist facies is constrained by reaction i2-(hb), which gives rise to the appearance of glaucophane, forming the typical paragenesis gl + ep of epidote blueschist

Fig. 5. (**a**) & (**b**) ACF diagrams, (**c**) *P–T* projection and (**d**) *P–T* pseudosections for the MORB compositions showing the phase relations under greenschist, amphibolite and blueschist facies. The univariant reactions are nominated with the absent phase. The diagnostic assemblage in each *P–T* field is shaded in yellow; the non-diagnostic assemblages are not shaded. Abbreviations of subfacies: ab-GS, albite greenschist; act-LAM, actinolite low-temperature amphibolite; ep-AM, epidote amphibolite; ep-BS, epidote blueschist; pl-GS, plagioclase greenschist; LAM, low-temperature amphibolite.

subfacies (ep-BS). According to the phase modelling in Figure 1, the appearance of glaucophane is immediately followed by the disappearance of albite. The ep-BS subfacies contains two assemblages: gl + ep + act and gl + ep + hb, with hornblende (actually barroisite) replacing actinolite through reaction i2-(chl) as the temperature rises.

Phase relations in the transition from blueschist to eclogite facies

The possible minerals present in metabasic rocks under blueschist and eclogite facies may include lawsonite, omphacite, glaucophane, hornblende, garnet, epidote and chlorite, with quartz, water and $NaAlO_2$ components being in excess. Actinolite and talc are predicted to be present for the *P–T* conditions of interest according to the phase modelling in Figure 1, which are not, however, major phases in natural low-temperature eclogites and blueschists under high pressures (e.g. Carswell 1990; Zhang *et al.* 2007; Wei *et al.* 2009). The above minerals construct three invariant assemblages: i3, i4 and i5 (Fig. 4; Table 3). The ACF plots for invariant assemblage

i3 are shown in Figure 6a, and the *P–T* projection that includes the distribution of univariant reactions and the possible diagnostic and non-diagnostic assemblages in each divariant field are shown in Figure 6b. For the MORB composition (M), the *P–T* pseudosection can be qualitatively obtained as shown in Figure 6c, where only one reaction – i3-(om) – cannot be seen by the composition. Thus, four *P–T* fields and, accordingly, four metamorphic subfacies, including lawsonite blueschist (law-BS), epidote blueschist (ep-BS), lawsonite eclogite (law-EC) and epidote eclogite (ep-EC), can be classified, each of which has a specific divariant assemblage (Fig. 6c).

If FeO and MgO are not regarded as one component (F) but two independent components and, moreover, Na_2O and Fe_2O_3 are also treated as independent components, as we did in the phase modelling in Figure 1, the ACF univariant reactions in Figure 6c will become multivariant continuous ones. For instance, glaucophane will not disappear on the univariant lines i3-(ep) and i3-(law) in Figure 6c, but will remain present in a wide *P–T* range until it is out, forming the transitional glaucophane–lawsonite eclogite (gl–law-EC) and glaucophane–epidote
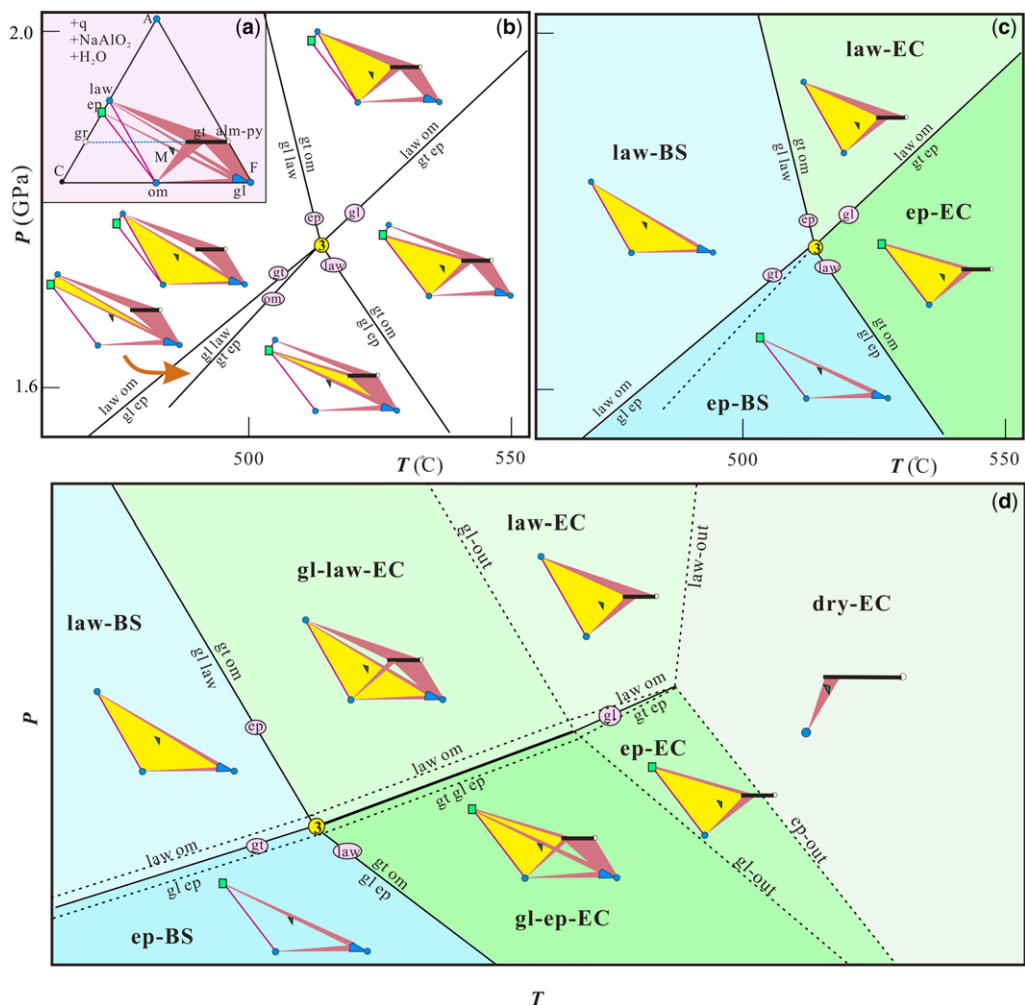
Fig. 6. (a) ACF diagram, (b) *P–T* projection and (c) & (d) *P–T* pseudosections for the MORB composition showing the phase relations under blueschist and eclogite facies. Abbreviations of subfacies: dry-EC, dry eclogite; ep-BS, epidote blueschist; ep-EC, epidote eclogite; gl–ep-EC, glaucophane–epidote eclogite; gl–law-EC, glaucophane–lawsonite eclogite; law-BS, lawsonite blueschist; law-EC, lawsonite eclogite. The other abbreviations are the same as those in Figures 4 and 5.

eclogite (gl–ep-EC) subfacies (Fig. 6d). The invariant assemblage i3 will also become a multivariant reaction (shown as a bold solid line in Fig. 6d). Accordingly, the univariant reactions i3-(gt) and i3-(gl) will also become continuous ones but in narrow *P–T* ranges (the dashed lines), according to the modelling results in Figure 1. For the law-EC and ep-EC subfacies assemblages in Figure 6d, the mode of lawsonite and epidote will decrease as garnet is enriched in grossular content with increasing *P–T* conditions. These two phases will disappear when the gt–om tieline passes through the projection of the MORBs (M), resulting in the formation of a dry eclogite (dry-EC)

subfacies assemblage consisting mainly of garnet and omphacite. Thus, seven subfacies of the eclogite and blueschist facies can be subdivided (Fig. 6d) if taking into account continuous reactions and variations in mineral compositions with a change in *P–T* conditions.

The ACF plots for invariant assemblages i4 and i5, and the *P–T* projections, are shown in Figure 7a–c. The *P–T* pseudosection for the MORB composition can be qualitatively analysed, as shown in Figure 7d. The reactions i4-(ep), i5-(hb) and i5-(ep) cannot be seen by the composition. Thus, four *P–T* fields, or four metamorphic subfacies

including ep-BS, ep-EC, ep-AM and gt–ep-AM (garnet–epidote amphibolite), can be classified, where the ep-BS subfacies includes two divariant assemblages but each of the other three subfacies has one divariant assemblage (Fig. 7d).

In a more realistic system, as we showed above, the ACF invariant assemblage and univariant reactions in Figure 7d will become multivariant. Especially, reactions i4-(hb) and i4-(gl), involving the stability of two amphiboles, will become continuous and maintain the presence of glaucophane and hornblende in a wide P–T range until they are out, forming the transitional gl–ep-EC and hb–ep-EC (hornblende–epidote eclogite) subfacies (Fig. 7e).
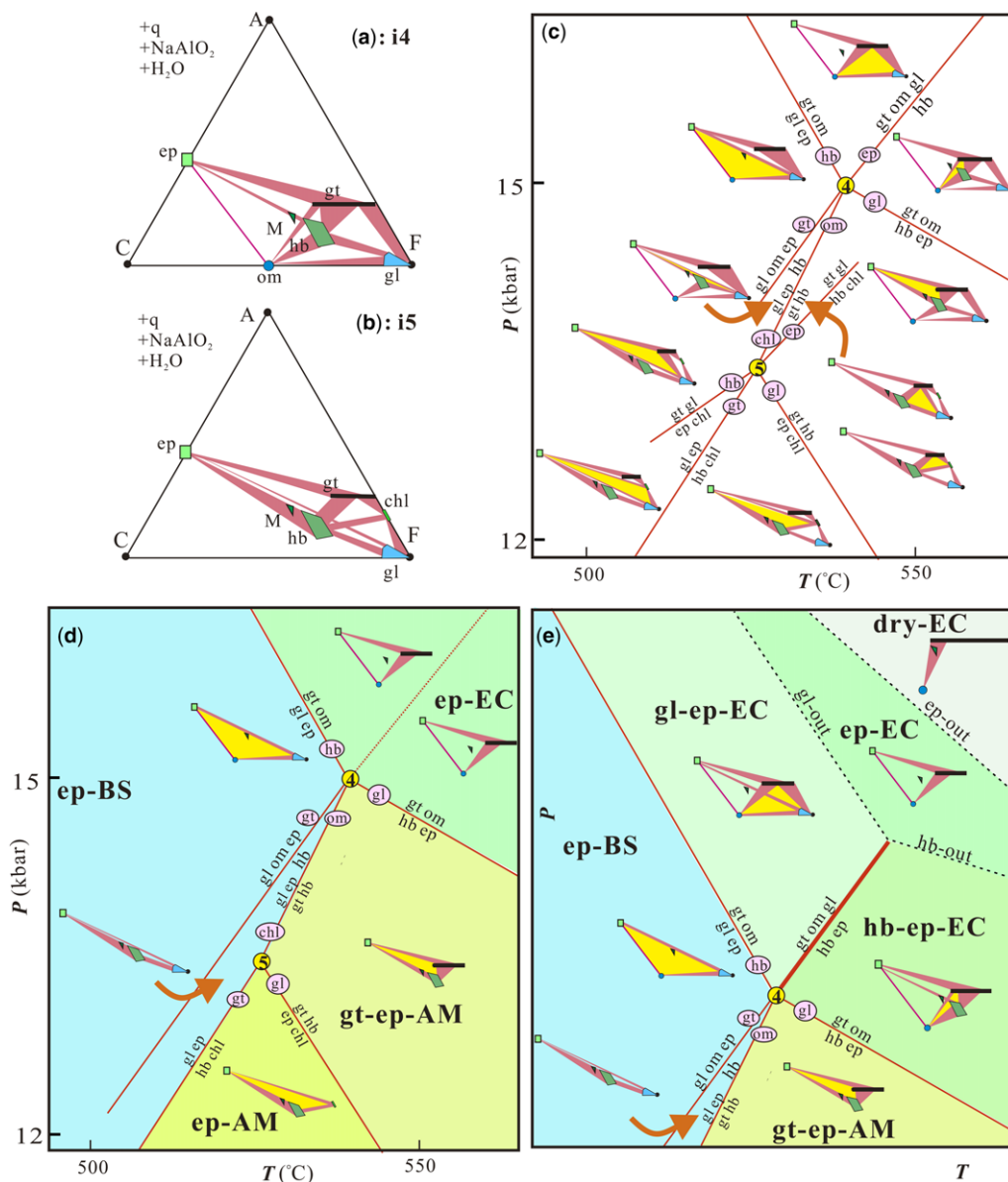
Fig. 7. (**a**) & (**b**) ACF diagrams, (**c**) P–T projection and (**d**) & (**e**) P–T pseudosections for the MORB composition showing the phase relations under blueschist and eclogite facies. Abbreviations of subfacies: gt–ep-AM, garnet–epidote amphibolite; hb–ep-EC, hornblende–epidote eclogite. The other abbreviations are the same as those in Figures 4 and 6.

The invariant assemblage i4 will become a multivariant reaction (shown as a bold solid line in Fig. 7e) responsible for the transformation between glaucophane and hornblende. Accordingly, the other ACF univariant tractions in Figure 7d will be also multivariant, but their changes are neglected in Figure 7e because they cannot form wide ranges of transitional subfacies according to the phase modelling in Figure 1. As garnet is enriched in grossular content with increasing $P–T$ conditions in the ep-EC subfacies, epidote will decrease in its mode and finally disappear when the gt–om tie-line passes through the projection of the MORB composition (M), resulting in the formation of the dry-EC subfacies.

Phase relations in the transition from amphibolite to granulite facies

The possible minerals present in metabasic rocks under amphibolite and granulite facies may include hornblende, diopside, orthopyroxene, garnet and plagioclase, with quartz, melt and $NaAlO_2$ component being in excess. The above minerals construct an invariant assemblage (i6) and their ACF plots are shown in Figure 8a. The possible univariant reactions in assemblage i6 are presented in Table 3 and the $P–T$ projections are shown in Figure 8b. For the MORB composition, the $P–T$ pseudosection can be qualitatively obtained as
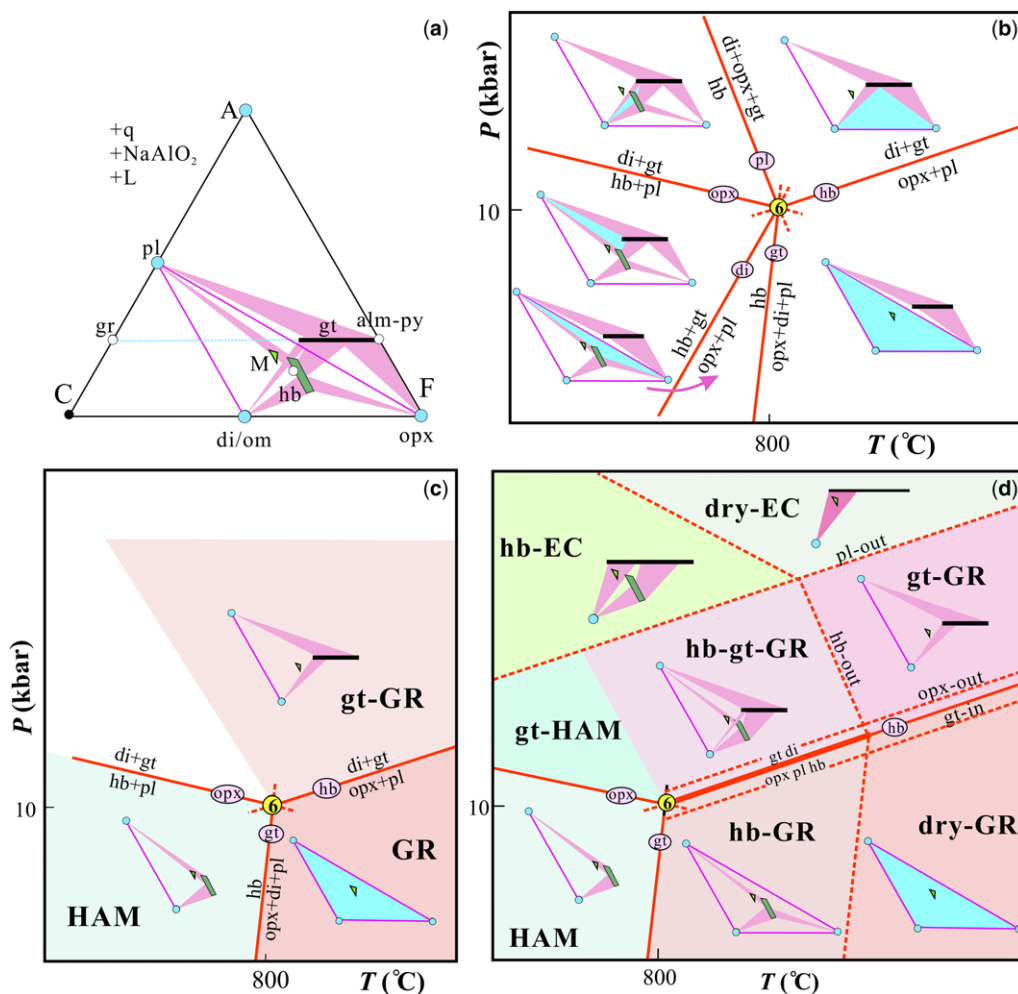
Fig. 8. (**a**) ACF diagram, (**b**) $P–T$ projection and (**c**) & (**d**) $P–T$ pseudosections for the MORB composition showing the phase relations under amphibolite, granulite and eclogite facies. Abbreviations of subfacies: dry-EC, dry eclogite; dry-GR, dry granulite; HAM, high-temperature amphibolite; hb-EC, hornblende eclogite; hb-GR, hornblende granulite; hb–gt-GR, hornblende–garnet granulite; gt-GR, garnet granulite; gt-HAM, garnet high-temperature amphibolite. The other abbreviations are the same as those in Figure 4.

shown in Figure 8c, where three reactions i6-(opx), i6-(hb) and i6-(gt) can be seen by the composition. Thus, three P–T fields and, accordingly, three metamorphic facies or subfacies including high-temperature amphibolite (HAM), granulite (GR) and garnet granulite (gt-GR) can be classified, each of which has a specific divariant assemblage (Fig. 8c).

If taking into account other non-ACF components, and regarding FeO and MgO as separately independent components, the invariant and univariant assemblages in Figure 8c will become multivariant continuous ones. For instance, the invariant assemblage i6 will become a multivariant reaction (shown as a bold solid line in Fig. 8d) until hornblende is out. The univariant reaction i6-(gt) becomes multivariant, with hornblende coexisting with opx + di + pl, forming the transitional assemblage of hornblende granulite (hb-GR) subfacies (Fig. 8d). For reaction i6-(opx), the assemblage hb + pl + gt + di can be stable in a wide P–T range of 9–15 kbar and 600–1000°C, as suggested from both experimental and modelling results (Figs 1 and 2), covering the P–T conditions of both amphibolite and granulite facies. As there will not be a clear boundary between these two facies that share one assemblage hb + pl + gt + di, we divide it into two subfacies: garnet high-temperature amphibolite (gt-HAM) and hornblende–garnet granulite (hb–gt-GR), according to whether the hornblende mode is less than or more than the mode of the anhydrous minerals of garnet and diopside (Wei *et al.* 2017). Thus, the gt-HAM subfacies is dominated by hydrous minerals (hornblende) and the hb–gt-GR subfacies is dominated by anhydrous minerals, although both of them have the same assemblage. Within this assemblage, garnet will be enriched in grossular content with increasing pressure, coupled with plagioclase decreasing in its mode and becoming enriched in albite and finally disappearing when the gt–di tie-line passes through the projection of bulk-rock composition (M). Meanwhile, clinopyroxene is becoming enriched in jadeite and transformed into omphacite, resulting in the formation of the hb-EC subfacies assemblage with om + gt + hb. The hb–gt-GR and hb-EC subfacies assemblages are transformed into the dry-EC and gt-GR subfacies after hornblende disappears with increasing P–T conditions. Moreover, the transition from the dry gt-GR subfacies to the dry-EC subfacies can occur after plagioclase is out with increasing pressure.

Reaction i6-(hb) also becomes multivariant with the assemblage opx + pl + gt + di stable in a small pressure range, as roughly displayed by the dashed lines in Figure 8d. If neglecting these assemblages as stable in narrow ranges, eight subfacies assemblages can be classified for metabasic rocks under suprasolidus conditions.

Phase relations in the transition from AM to EC facies

The possible minerals present in metabasic rocks under amphibolite and eclogite facies may include hornblende, diopside/omphacite, epidote, garnet, plagioclase and chlorite, with quartz, H_2O and $NaAlO_2$ components being in excess. They construct two invariant assemblages (i7 and i8). The ACF plots and P–T projection are shown in Figure 9a–c. For the MORB composition, the P–T pseudosection can be qualitatively obtained as shown in Figure 9d. Six P–T fields and, accordingly, six metamorphic subfacies including ep-AM, gt–ep-AM, LAM, HAM, ep-EC and gt-GR can be classified, each of which has a specific divariant assemblage (Fig. 9c). If you take into account other non-ACF components, and regard FeO and MgO as separately independent components, the invariant and univariant assemblages in Figure 9d will become multivariant continuous ones. If we just consider the multivariant natures of reactions i7-(di) and i7-(ep), two transitional assemblages of hb + pl + gt + ep and hb + pl + gt + di are produced after garnet appears (Fig. 9e), which are nominated as the garnet-low-temperature amphibolite (gt-LAM) and garnet high-temperature amphibolite (gt-HAM) subfacies, respectively. Accordingly, invariant assemblage i7 will become multivariant with the five phases stable in a small P–T range, which is also grouped into the gt-LAM subfacies in Figure 9e. With increasing pressure, plagioclase in the gt-LAM and gt-HAM subfacies will decrease in mode and finally disappear, concomitant with garnet becoming enriched in grossular, resulting in the formation of three subfacies assemblages of gt–ep-AM, hb–ep-EC and hb-EC. As hornblende has wide stability fields, as suggested in Figures 1 and 2, the hornblende-absent ep-EC and gt-GR assemblages will not be present in the P–T range of interest.

Phase relations for kyanite-bearing eclogitic assemblages

Kyanite-bearing eclogitic assemblages may include garnet, diopside/omphacite, epidote, lawsonite, plagioclase and kyanite, with quartz, H_2O and $NaAlO_2$ components being in excess. They construct two invariant assemblages (i9 and i10), and their ACF plots and P–T projection are shown in Figure 10a–c. Two AC subsystem reactions, involving law = ep + ky (i9-(om) and i9-(gt)) and pl = ep + ky (i10-(om) and i10-(gt)), are present that bound the maximum stabilities of lawsonite and plagioclase (anorthite), respectively. Both of them cannot be seen by the MORB composition (Fig. 10d). Thus, four P–T fields or four metamorphic subfacies, including law-EC, ep-EC, ky-EC (kyanite eclogite) and
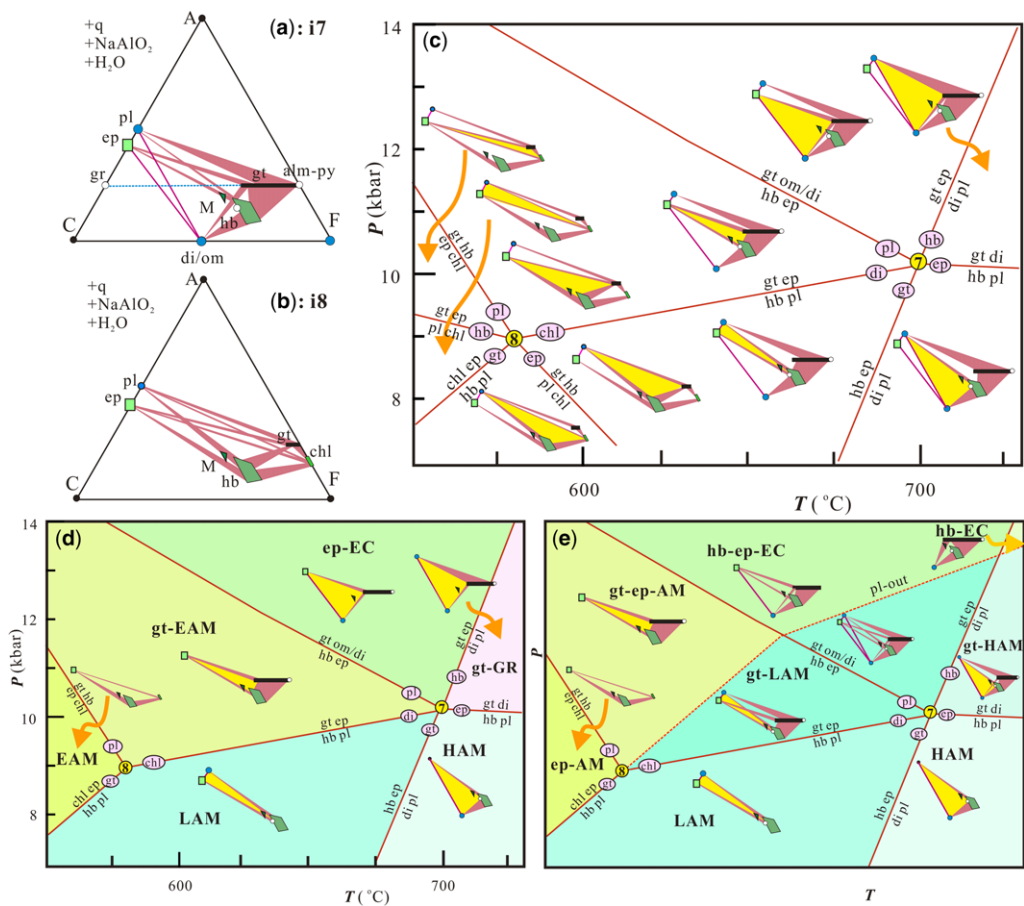
Fig. 9. (**a**) & (**b**) ACF diagrams, (**c**) *P*–*T* projection and (**d**) & (**e**) *P*–*T* pseudosections for the MORB composition showing the phase relations under amphibolite and eclogite facies. Abbreviations of subfacies: hb–ep-EC, hornblende–epidote eclogite; gt-LAM, garnet low-temperature amphibolite. The other abbreviations are the same as those in Figures 4, 5 and 8.

gt-GR, can be classified (Fig. 10d). If the other components are considered in a more realistic system, the univariant reactions will become multivariant. For instance, a transitional assemblage gt + om + law + ky will appear between the law-EC and ky-EC subfacies assemblages; and a transitional assemblage gt + om + ep + ky between the ep-EC and ky-EC subfacies assemblages. If you take into account the wide stability of hornblende (e.g. 22–23 kbar/700–800°C in Fig. 2), the phase relations defined by i10 are mostly not present in basic rocks. For instance, the gt-GR subfacies may be replaced by a gt-HAM assemblage (Fig. 8), and the ep-EC subfacies under *P* < 23 kbar is substituted by the hb–ep-EC and gt-LAM subfacies assemblages (Figs 7 & 9). In fact, kyanite-bearing eclogites are stable in the *P*–*T* conditions of >20 kbar and >600°C (Holland & Powell 1998; Wei et al. 2003). In addition, kyanite

in the ky-EC assemblage in Figure 10 may disappear due to garnet becoming enriched in grossular with increasing *P*–*T* conditions. In many cases, kyanite in UHP eclogites was interpreted to have been formed during decompression, which is absent in the UHP peak stage (e.g. Wei et al. 2010, 2013). Thus, kyanite-bearing eclogitic assemblages are generally stable in small *P*–*T* ranges (see Fig. 1) or commonly absent, and were neglected in the following discussions.

A complete *P*–*T* pseudosection for MORBs from the ACF analysis

On the basis of the phase relations analysed above, a complete *P*–*T* pseudosection is presented in Figure 11. It includes 22 subfacies assemblages in

PHASE RELATIONS IN METABASIC ROCKS
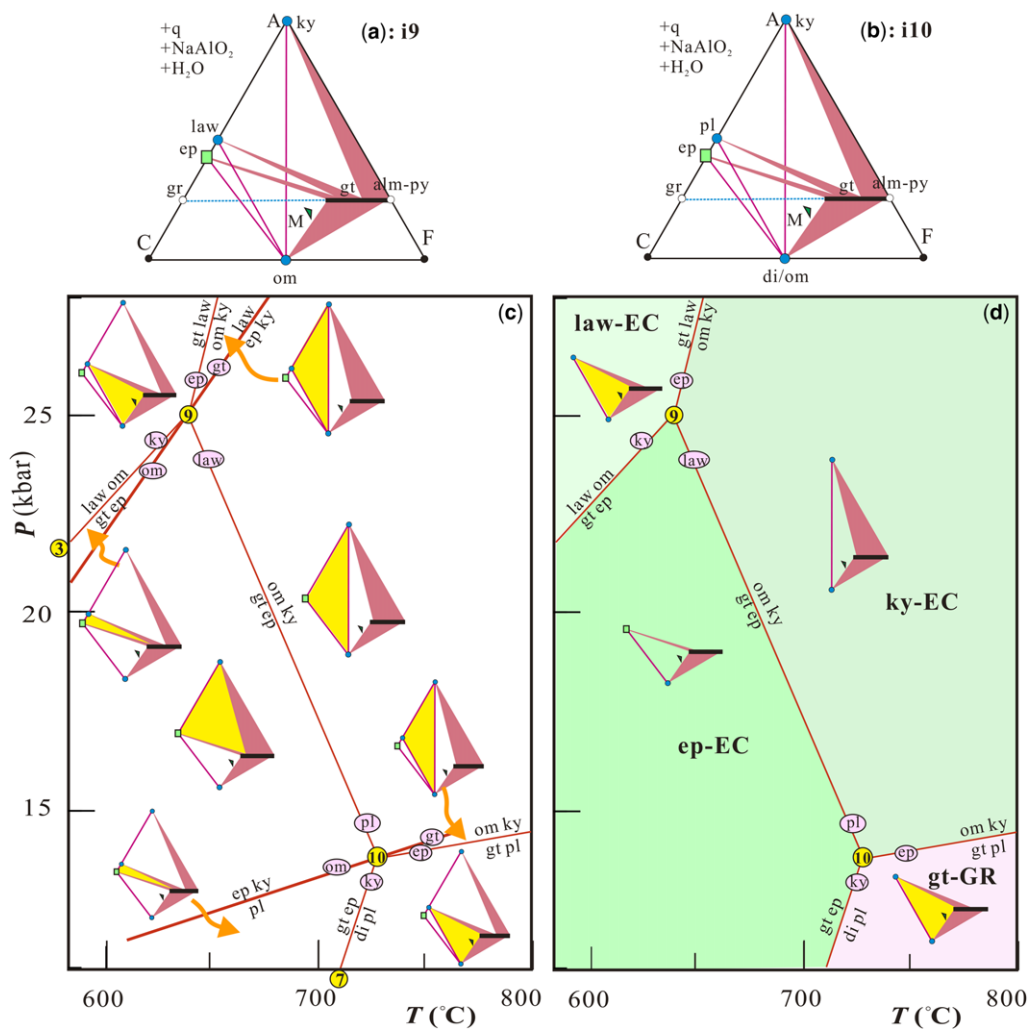
Fig. 10. (**a**) & (**b**) ACF diagrams, (**c**) *P–T* projection and (**d**) *P–T* pseudosection for the MORB composition showing the phase relations in the kyanite-bearing eclogitic assemblages. Abbreviations of subfacies: ky-EC, kyanite eclogite. The other abbreviations are the same as those in Figures 4 and 6.

the *P–T* range of 0–32 kbar and 400–1100°C. The boundaries between these subfacies assemblages are defined by ACF invariant reactions (i3, i4 and i6; shown as bold solid lines), univariant reactions (solid lines) and continuous reactions, involving hb-out, gl-out, pl-out, law-out and ep-out, which are shown as dashed lines.

The phase relations in Figure 11 are controlled by the stabilities of garnet, plagioclase, hornblende, glaucophane, epidote and lawsonite. Garnet is stable in the high *P–T* fields of >9–10 kbar and >450°C in Figure 11. Garnet-forming (gt-in) reactions show flat slopes in temperatures above point i8 controlled by the reactions consuming hb + pl and opx + pl, but

vertical slopes in temperatures below point i8 involving reactions at the expense of ep + chl, gl + ep and gl + law. Phase modelling in Figure 1 shows that the garnet-in curves under low-temperature conditions are closely related to the chlorite-out, suggesting that chlorite should be involved in the garnet-forming reactions. Garnet stabilities will be widened to lower *P–T* conditions to consider MnO as an independent component in the system (Mahar *et al.* 1997; Wei *et al.* 2004), and beyond the limits presented in Figure 11, which, however, can be regarded as the boundaries that indicate the presence of a considerable amount (>5–10 vol%) of garnet (Tian & Wei 2014) in rocks.
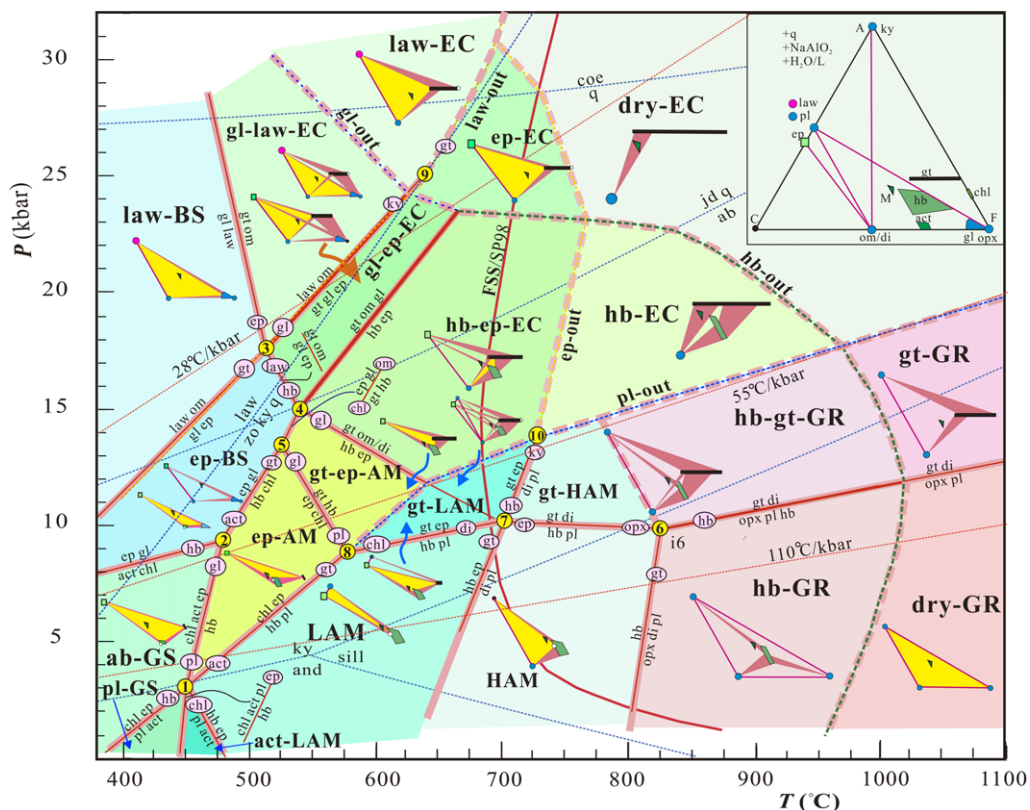
Fig. 11. A complete pseudosection for the MORB compositions in Table 2 showing the stabilities of 22 subfacies assemblages in five metamorphic facies. The greenschist facies include two subfacies: albite greenschist (ab-GS) and plagioclase greenschist (pl-GS). The amphibolite facies include seven subfacies: actinolite low-temperature amphibolite (act-LAM), low-temperature amphibolite (LAM), high-temperature amphibolite (HAM), epidote amphibolite (ep-AM), garnet–epidote amphibolite (gt–ep-AM), garnet low-temperature amphibolite (gt-LAM) and garnet high-temperature amphibolite (gt-HAM). The granulite facies include four subfacies: hornblende granulite (hb-GR), dry granulite (dry-GR), hornblende–garnet granulite (hb–gt-GR) and garnet granulite (gt-GR). The blueschist facies include two subfacies: epidote blueschist (ep-BS) and lawsonite blueschist (law-BS). The eclogite facies include seven subfacies: glaucophane–lawsonite eclogite (gl–law-EC), glaucophane–epidote eclogite (gl–ep-EC), hornblende–epidote eclogite (hb–ep-EC), lawsonite eclogite (law-EC), epidote eclogite (ep-EC), hornblende eclogite (hb-EC) and dry eclogite (dry-EC). The boundaries between these subfacies assemblages are defined by the ACF invariant reactions (i3, i4 and i6: thick solid lines), univariant reactions (thin solid lines) and continuous reactions (dashed lines). The ACF diagram in the upper right-hand corner shows the plots of minerals in metabasic rocks. The apparent geothermal gradients of 110°C/kbar, 55°C/kbar and 28°C/kbar that cause the four-fold classification of metamorphism in this study are shown as dashed red lines. The others are the same as in Figures 1 and 2.

Plagioclase is stable in the low-pressure fields in Figure 11, and its disappearance reactions show moderately positive slopes (i.e. at about 5 kbar/ 500°C and 10 kbar/600°C) defined by ACF univariant reactions consuming actinolite and hornblende in temperatures below point i8, but show gently positive slopes (i.e. at about 15 kbar/800°C and 20 kbar/1100°C) in temperatures above point i8, constrained by the ACF continuous reactions as a result of the coexisting garnet becoming enriched in grossular.

Hornblende is stable in the lower-central part of Figure 11 at <24 kbar and 420–1000°C, and its formation is defined by the ACF univariant reactions at the expense of chl + act + pl, chl + act + ep and ep + gl under pressures below 15 kbar (i4), and an ACF invariant reaction (i4), gt + om + gl = hb + ep. At higher temperatures above 660°C, hornblende-out is controlled by the ACF continuous reactions with the formation of garnet, omphacite/diopside and orthopyroxene. Glaucophane is stable in the low-temperature (<650°C) and high-pressure (>8 kbar)

part of Figure 11. Its disappearance is controlled by the ACF univariant reactions consuming epidote and producing act + chl, hb + chl and gt + hb at pressures below 15 kbar (i4), the ACF invariant reaction (i4) to produce hornblende at pressures between 15 and 24 kbar, and the ACF univariant reactions including gl + law/ep = gt + om at the higher pressures >24 kbar.

Lawsonite appears in the low-temperature (<700°C) and high-pressure (>10 kbar) conditions in Figure 11. Its disappearance is controlled by the ACF univariant reactions consuming omphacite in pressures below 25 kbar (i9), and by ACF continuous reactions resulted from the coexisting garnet becoming enriched in grossular. Epidote appears in the P–T conditions of <30 kbar and < 750°C in Figure 11. Its low-temperature limits are defined by the law-out reactions, and its high-temperature limits are defined by the ACF continuous reactions consuming hb + ep and gt + ep, and producing di + pl in the plagioclase stability fields of pressures below i10, and by the ACF continuous reactions in higher pressures above i10.

A four-fold classification of metamorphism

Miyashiro (1961, 1994) proposed the three-fold classification of metamorphism including the low-, medium- and high-P/T types with average geothermal gradients approximately >35°C/km, between 35 and 15°C/km, and <15°C/km, respectively. As the values of geothermal gradient vary with the average density of crustal and mantle rocks used in the calculation, and, also, the pressure values recovered for metamorphic rocks do not simply reflect the depth of crust, Brown (2007) preferred to use apparent thermal gradients for the classification of metamorphism. On the basis of the summary of P–T conditions from 140 metamorphic belts in the world, he proposed three types of metamorphism as: the high-pressure–ultrahigh-pressure metamorphism (HPM–UHPM) group; the medium-temperature eclogite and high-pressure granulite group (E-HPGM) group; and the granulite–ultrahigh temperature (G–UHTM) group, with apparent thermal gradients of 150–350°C/GPa, 350–750°C/GPa and 750–1500°C/GPa, respectively. Following these ideas and on the basis of the phase relations presented in Figure 11, we propose a four-fold classification of metamorphism, including low-, medium-, high- and very-high-P/T types. The average apparent geothermal gradients that cause these four types of metamorphism are approximately >110°C/kbar for the low-P/T type, between 110 and 55°C/kbar for the medium-P/T type, between 55 and 28°C/kbar for the high-P/T type, and <28°C/kbar for the very-high-P/T type.

The very-high-P/T type of metamorphism mainly occurs in the lawsonite stability fields, with geothermal gradients corresponding to the tectonic settings for the cold subduction of oceanic slabs (e.g. Peacock & Wang 1999; Tsujimori et al. 2006; Song et al. 2007; Tsujimori & Ernst 2014; Wei & Tian 2015) and continental crust (e.g. Wei et al. 2010, 2013). Progressive metamorphic evolution with increasing P–T conditions is dominated by the dehydration of hydrous phases of lawsonite and glaucophane. As shown in Figure 11, the paragenesis of law + gl constructs the typical assemblage of the law-BS subfacies, which gives rise to the eclogitic assemblage of gt + om. With increasing P–T conditions, the eclogitization is dominated by the ACF univariant reaction with the formation of gt + om and the consumption of gl + law (reaction i3-(ep)), which can occur continuously in a wide P–T range (gl–law-EC subfacies) until glaucophane is out. The following evolution is controlled by lawsonite dehydration in the ACF divariant assemblage law–gt–om (law-EC subfacies), which is attributed to garnet becoming enriched in grossular with increasing in the P–T conditions. After lawsonite is out, the only hydrous phase in the metabasic rocks is phengite, which may disappear when P–T conditions cross the water-saturated solidus (Schmidt et al. 2004) with sufficient water.

The high-P/T type of metamorphism mainly occurs in the epidote and hornblende stability fields above the high-pressure limits of plagioclase, with geothermal gradients corresponding to the tectonic settings for the warm subduction of oceanic slabs (e.g. Peacock & Wang 1999) and the deep part of continental thickening belts: for instance, at the Himalaya (e.g. Wang et al. 2017) and the Belomorian Mobile Belt (e.g. Perchuk & Morgunova 2014). Progressive metamorphic evolution with increasing P–T conditions is dominated by the dehydration of hydrous phases of epidote, glaucophane and hornblende. If starting from the ep-BS subfacies characteristic of the paragenesis of ep + gl, the subsequent metamorphic evolution or eclogitization in the P–T conditions above invariant point i4 is dominated by the ACF univariant reaction with the formation of gt + om and the consumption of gl + ep (reaction i3-(law) or i4-(hb)), which can occur continuously in a wide P–T range (gl–ep-EC subfacies) until glaucophane is out. Further eclogitization in the ACF divariant fields of the ep-EC subfacies is controlled by epidote dehydration due to garnet becoming enriched in grossular. For progressive changes with increasing P–T conditions below point i4, the ep-BS assemblage gives rise to the assemblages of gt + hb + ep in the gt–ep-AM subfacies and hb + ep + chl in the ep-AM subfacies, respectively. Further evolution is controlled by the ACF univariant (i4-(gl)) hb + ep = gt + om, which proceeds in a

wide P–T range of hb–ep-EC subfacies until hornblende is out when the pressure is above $c.$ 23 kbar or until epidote is out when the temperature is above $c.$ 750°C. For the latter case, the subsequent metamorphic evolution occurs in the P–T field of the hb-EC subfacies dominated by the ACF divariant reaction hb = gt + om until hornblende disappears, resulting in the formation of the dry-eclogite subfacies assemblage.

The medium-P/T type of metamorphism mainly occurs in the plagioclase stability fields, with geothermal gradients corresponding to the tectonic settings for collisional orogenic belts (Miyashiro 1994). Progressive metamorphic evolution is controlled by dehydration reactions i1-(pl) and i1-(act), with the formation of hornblende in the ab-GS and ep-AM subfacies. Further evolution in the garnet-absent fields is dominated by hornblende dehydration reactions including i7-(gt) and i6-(gt) until hornblende is out at $c.$ 1000°C, forming the LAM, HAM, hb-GR and dry-GR subfacies assemblages. The metamorphic evolution in the garnet-present fields is dominated by the dehydration of hornblende and epidote in the gt-LAM subfacies, followed by hornblende dehydration in the gt-HAM and hb–gt-GR subfacies assemblages.

The low-P/T type of metamorphism, equivalent to that in Miyashiro (1994), with geothermal gradients corresponding to the tectonic settings for island arcs, continental rift, oceanic ranges and contact aureoles (Miyashiro 1994). Progressive metamorphic evolution is characterized by the formation of the pl-GS and act-LAM subfacies assemblages, and the subsequent evolution is controlled by hornblende dehydration, similar to that in the medium-P/T type.

As temperature is above the fluid-saturated solidus, the dehydration of hydrous phases will result in anatexis in metabasic rocks, producing granitic or trondhjemitic–tonalitic melts. Both phase-modelling and experimental data (e.g. Schmidt et al. 2004) suggest that K_2O phases (biotite and muscovite) are consumed on or just above the fluid-saturated solidus. At 10–28 kbar, epidote is stable at suprasolidus conditions, and its dehydration can produce small amount of melt (<3 mol%) according to the modelling in Wei et al. (2017). The melting of metabasic rocks is dominated by the dehydration of hornblende, which occurs at HAM, hb-GR, gt-HAM, hb–gt-GR and hb-EC subfacies. Phase-modelling results suggest that the experimentally defined fluid-absent solidi of amphibolite ranging from 800 to 850°C in Figure 2 (e.g. Rushmer 1991; Winther & Newton 1991) are not really present, and could be regarded as effective solidi of metabasic rocks with quite a bit of melt that can be observed (Wei et al. 2017). The melting of basic assemblages saturated with water should have started from the fluid-saturated solidus because the progressive evolution under subsolidus conditions

may continuously release fluids, and so the rocks are always under fluid-present conditions for a natural progressive evolution.

Concluding remarks

Quantitative phase modelling using available thermodynamic datasets, software and mixing models for relevant phases have been proved to be effective for elucidating the phase relations or metamorphic evolution for natural rocks (Powell et al. 1998; Holland & Powell 2011). Pseudosections calculated for most basic rocks can provide results comparable with those from experimental results, including the stability limits for lawsonite, epidote, amphibole, plagioclase and garnet. The phase relations in most P–T pseudosections for metabasic rocks look to be very complicated, but can be greatly simplified when viewed using ACF analysis. ACF composition–paragenesis diagrams are very useful not only for summarizing the results of petrographical work, but also for the purpose of the definition and characterization of individual metamorphic facies or subfacies; although it is now clear that they have too many defects to be used in rigorous thermodynamic discussions (Miyashiro 1994). On the basis of ACF composition–paragenesis diagrams, P–T projections that include all the phase relations in the ACF compositional space can be constructed following Schreinemakers' rules, and, thus, P–T pseudosections can be obtained for specific compositions. These qualitative P–T pseudosections are useful for understanding the complicated phase relations of metabasic rocks.

On the basis of ACF analysis, five metamorphic facies and 22 subfacies assemblages can be identified for metabasic rocks of MORB composition if the kyanite-bearing assemblages are neglected. The subfacies assemblages are mostly divariant, six are univariant and one is trivariant. All of the univariant subfacies assemblages resulted from the wide stability of hornblende and glaucophane.

A four-fold classification of metamorphism is presented on the basis of the phase relations in the qualitative P–T pseudosections for metabasic rocks of MORB composition, including low-, medium-, high- and very-high-P/T types, where the low- and medium-P/T types are consistent with the stability fields of plagioclase, the very-high-P/T type is consistent with the stability fields of lawsonite, and the high-P/T type corresponds to the fields in-between the stability limits of lawsonite and plagioclase. The low- and medium-P/T types are similar to those in Miyashiro (1994), but the high- and very-high-P/T types seem to be subdivisions of the high-P/T type in Miyashiro (1994). This subdivision is necessary because the phase relations in the plagioclase-absent

fields are very complicated and suggest diverse tectonic settings, which cannot be included in one particular P/T type of metamorphism.

References

BEARD, J.S. & LOFGREN, G.E. 1991. Dehydration melting and water-saturated melting of basaltic and esitic greenstones and amphibolites at 1, 3 and 6.9 kbar. *Journal of Petrology*, **32**, 365–401.

BROWN, M. 2007. Metamorphic conditions in orogenic belts: a record of secular change. *International Geological Review*, **49**, 193–234.

BROWN, M. 2014. The contribution of metamorphic petrology to understanding lithosphere evolution and geodynamics. *Geoscience Frontiers*, **5**, 553–569.

CARSON, C.J., POWELL, R. & CLARKE, G.L. 1999. Calculated mineral equilibria for eclogites in CaO–Na2O–FeO–MgO–Al2O3–SiO2–H2O: application to the Pouébo Terrane, Pam Peninsula, New Caledonia. *Journal of Metamorphic Geology*, **17**, 9–24.

CARSWELL, D.A. 1990. Eclogites and the eclogite facies: definitions and classification. *In*: CARSWELL, D.A. (ed.) *Eclogite Facies Rocks*. Blackie, Glasgow, 1–13.

CLEMENS, J.D. & VIELZEUF, D. 1987. Constraints on melting and magma production in the crust. *Earth and Planetary Science Letters*, **86**, 287–306.

CONNOLLY, J.A.D. 1990. Multivariable phase diagrams; an algorithm based on generalized thermodynamics. *American Journal of Science*, **290**, 666–718.

CONNOLLY, J.A.D. 2005. Computation of phase equilibria by linear programming: a tool for geodynamic modelling and its application to subduction zone decarbonation. *Earth and Planetary Science Letters*, **236**, 524–541.

DALE, J., POWELL, R., WHITE, R.W., ELMER, F. & HOLLAND, T.J.B. 2005. A thermodynamic model for Ca–Na clinoamphiboles in Na2O–CaO–FeO–MgO–Al2O3–SiO2–H2O–O for petrological calculations. *Journal of Metamorphic Geology*, **23**, 771–791.

DE CAPITANI, C. 1994. Gleichgewichts-Phasendiagramme: theorie und software. *Berichte der Deutschen Mineralogischen Gesellschaft*, **6**, 48.

DE CAPITANI, C. & BROWN, T.D. 1987. The computation of chemical equilibrium in complex systems containing non-ideal solutions. *Geochimica et Cosmochimica Acta*, **51**, 2639–2652.

DE CAPITANI, C. & PETRAKAKIS, K. 2010. The computation of equilibrium assemblage diagrams with Theriak/Domino software. *American Mineralogist*, **95**, 1006–1016.

DIENER, J.F.A. & POWELL, R. 2012. Revised activity–composition models for clinopyroxene and amphibole. *Journal of Metamorphic Geology*, **30**, 131–142.

DIENER, J.F.A., POWELL, R., WHITE, R.W. & HOLLAND, T.J.B. 2007. A new thermodynamic model for clino- and orthoamphiboles in the system Na2O–CaO–FeO–MgO–Al2O3–SiO2–H2O–O. *Journal of Metamorphic Geology*, **25**, 631–656.

ENGEL, A.E.J., ENGEL, C.G. & HAVENS, R.G. 1965. Chemical characteristics of oceanic basalts and the upper mantle. *Geological Society of America Bulletin*, **76**, 719–734.

ESKOLA, P. 1915. *On the Relations Between the Chemical and Mineralogical Composition in the Metamorphic Rocks of the Orijarvi Region*. Bulletin de la Commission Géologique de Finlande, **44**.

ESKOLA, P. 1939. Die metamorphen Gesteine. *In*: BARTH, T.F.W., CORRENS, C.W. & ESKOLA, P. (eds) *Die Entstehung der Gesteine; Ein Lehrbuch der Petrogenese*. Springer, Berlin, 263–407.

GALE, A., DALTON, C.A., LANGMUIR, C.H., SU, Y.J. & SCHILLING, J.G. 2013. The mean composition of ocean ridge basalts. *Geochemistry, Geophysics, Geosystems*, **14**, 489–518.

GREEN, D.H. & RINGWOOD, A.E. 1967. An experimental investigation on the gabbro to eclogite transformation and its petrological applications. *Geochimica et Cosmochimica Acta*, **31**, 767–833.

GREEN, E.C.R., HOLLAND, T.J.B. & POWELL, R. 2007. An order–disorder model for omphacitic pyroxenes in the system jadeite–diopside–hedenbergite–acmite, with applications to eclogitic rocks. *American Mineralogist*, **92**, 1181–1189.

GREEN, E.C.R., WHITE, R.W., DIENER, J.F.A., POWELL, R., HOLLAND, T.J.B. & PALIN, R.M. 2016. Activity–composition relations for the calculation of partial melting equilibria for metabasic rocks. *Journal of Metamorphic Geology*, **34**, 845–869.

GREEN, T.H. 1967. An experimental investigation of sub-solidus assemblages formed at high pressure in high-alumina basalt, kyanite eclogite and grosspydite compositions. *Contributions to Mineralogy and Petrology*, **16**, 84–114.

GUIRAUD, M., HOLLAND, T. & POWELL, R. 1990. Calculated mineral equilibria in the greenschist–blueschist–eclogite facies in Na2O–FeO–MgO–Al2O3–SiO2–H2O. *Contributions to Mineralogy and Petrology*, **104**, 85–98.

HACKER, B.R., ABERS, G.A. & PEACOCK, S.M. 2003. Subduction factory 1. Theoretical mineralogy, densities, seismic wave speeds, and H2O contents. *Journal of Geophysical Research: Solid Earth*, **108**, 2029.

HACKER, B.R., GERYA, T.V. & JANE, A. 2013. Formation and exhumation of ultrahigh-pressure terranes. *Elements*, **9**, 289–293.

HASTIE, A.R., FITTON, J.G., BROMILEY, G.D., BUTLER, I.B. & ODLING, N.W.A. 2016. The origin of Earth's first continents and the onset of plate tectonics. *Geology*, **44**, G38226.1.

HOLLAND, T.J.B. & POWELL, R. 1990. An enlarged and updated internally consistent thermodynamic dataset with uncertainties and correlations: the system K2O–Na2O–CaO-MgO–MnO–FeO–Fe2O3–Al2O3–TiO2–SiO2–C–H2–O2. *Journal of Metamorphic Geology*, **8**, 89–124.

HOLLAND, T.J.B. & POWELL, R. 1998. An internally consistent thermodynamic data set for phases of petrological interest. *Journal of Metamorphic Geology*, **16**, 309–343.

HOLLAND, T.J.B. & POWELL, R. 2011. An improved and extended internally consistent thermodynamic dataset for phases of petrological interest, involving a new equation of state for solids. *Journal of Metamorphic Geology*, **29**, 333–383.

LAMBERT, I.B. & WYLLIE, P.J. 1972. Melting of gabbro (quartz eclogite) with excess water to 35 kilobars, with geological applications. *Journal of Geology*, **80**, 693–708.

LEAKE, B.E., WOOLLEY, A.R. ET AL. 1997. Nomenclature of amphiboles: report of the Subcommittee on Amphiboles of the International Mineralogical Association, Commission on New Minerals and Mineral Names. *American Mineralogist*, **82**, 1019–1037.

LIU, J., BOHLEN, S.R. & ERNST, W.G. 1996. Stability of hydrous phases in subducting oceanic crust. *Earth and Planetary Science Letters*, **143**, 161–171.

MAHAR, E.M., BAKER, J.M., POWELL, R., HOLLAND, T.J.B. & HOWELL, N. 1997. The effect of Mn on mineral stability in metapelites. *Journal of Metamorphic Geology*, **15**, 223–238.

MIYASHIRO, A. 1961. Evolution of metamorphic belts. *Journal of Petrology*, **2**, 277–311.

MIYASHIRO, A. 1994. *Metamorphic Petrology*. Oxford University Press, New York.

MOYEN, J. & STEVENS, G. 2006. Experimental constraints on TTG petrogenesis: implications for Archean geodynamics. *In*: BENN, K., MARESCHAL, J. & CONDIE, K.C. (eds) *Archean Geodynamics and Environments*. American Geophysical Union, Geophysical Monographs, **164**, 149–175.

PALIN, R.M., WHITE, R.W. & GREEN, E.C.R. 2016a. Partial melting of metabasic rocks and the generation of tonalitic–trondhjemitic–granodioritic (TTG) crust in the Archaean: constraints from phase equilibrium modelling. *Precambrian Research*, **287**, 73–90.

PALIN, R.M., WHITE, R.W., GREEN, E.C.R., DIENER, J.F.A., POWELL, R. & HOLLAND, T.J.B. 2016b. High-grade metamorphism and partial melting of basic and intermediate rocks. *Journal of Metamorphic Geology*, **34**, 871–892.

PEACOCK, S.M. & WANG, K. 1999. Seismic consequences of warm v. cool subduction metamorphism: examples from southwest and northeast Japan. *Science*, **286**, 937–939.

PERCHUK, A & MORGUNOVA, A.A. 2014. Variable P–T paths and HP–UHP metamorphism in a Precambrian terrane, Gridino, Russia: petrological evidence and geodynamic implications. *Gondwana Research*, **25**, 614–629.

POWELL, R. & HOLLAND, T. 1988. An internally consistent dataset with uncertainties and correlations, 3. Applications to geobarometry, worked examples and a computer program. *Journal of Metamorphic Geology*, **7**, 465–483.

POWELL, R. & HOLLAND, T.J.B. 1990. Calculated mineral equilibria in the pelite system, KFMASH (K_2O–FeO–MgO–Al_2O_3–SiO_2–H_2O). *American Mineralogist*, **75**, 367–380.

POWELL, R., HOLLAND, T. & WORLEY, B. 1998. Calculating phase diagram involving solid solutions via non-linear equations, with examples using THERMOCALC. *Journal of Metamorphic Geology*, **16**, 577–586.

QIAN, Q. & HERMANN, J. 2013. Partial melting of lower crust at 10–15 kbar: constraints on adakite and TTG formation. *Contributions to Mineralogy and Petrology*, **165**, 1195–1224.

RAPP, R.P. & WATSON, E.B. 1995. Dehydration melting of metabasalt at 8–32 kbar: implications for continental growth and crust–mantle recycling. *Journal of Petrology*, **36**, 891–931.

RAPP, R.P., WATSON, E.B. & MILLER, C.F. 1991. Partial melting of amphibolite/eclogite and the origin of Archaean trondhjemites and tonalites. *In*: HAAPALA, I. & CONDIE, K.C. (eds) Precambrian Granitoids Petrogenesis, Geochemistry and Metallogeny. *Precambrian Research*, **51**, 1–25.

RAPP, R.P., SHIMIZU, N. & NORMAN, M.D. 2003. Growth of early continental crust by partial melting of eclogite. *Nature*, **425**, 605–609.

REBAY, G., POWELL, R. & DIENER, J.F.A. 2010. Calculated phase equilibria for a MORB composition in a *P–T* range, 450–650°C and 18–28 kbar: the stability of eclogite. *Journal of Metamorphic Geology*, **28**, 635–645.

RUSHMER, T. 1991. Partial melting of two amphibolites: contrasting experimental results under fluid-absent conditions. *Contributions to Mineralogy and Petrology*, **107**, 41–59.

RUSHMER, T. 1993. Experimental high-pressure granulites: Some applications to natural mafic xenolith suites and Archean granulite terranes. *Geology*, **21**, 411–414.

SCHMIDT, M.W. & POLI, S. 1998. Experimentally based water budgets for dehydrating slabs and consequences for arc magma generation. *Earth and Planetary Science Letters*, **163**, 361–379.

SCHMIDT, M.W., VIELZEUF, D. & AUZANNEAU, E. 2004. Melting and dissolution of subducting crust at high pressures: the key role of white mica. *Earth and Planetary Science Letters*, **228**, 65–84.

SEN, C. & DUNN, T. 1994. Dehydration melting of a basaltic composition amphibolite at 1.5 and 2.0 GPa: implications for the origin of adakites. *Contributions to Mineralogy and Petrology*, **117**, 394–409.

SONG, S.G., ZHANG, L.F., NIU, Y.L., WEI, C.J., LIOU, J.G. & SHU, G.M. 2007. Eclogite and carpholite-bearing metapelite in the North Qilian suture zone, NW China: implications for Palaeozoic oceanic subduction. *Journal of Metamorphic Geology*, **25**, 547–563.

SUN, S.-s. & MCDONOUGH, W.F. 1989. Chemical and isotopic systematics of oceanic basalts: implications for mantle compositions and processes. *In*: SAUNDERS, A & NORRY, M. (eds) *Magmatism in the Ocean Basins*. Geological Society, London, Special Publications, **42**, 313–345, https://doi.org/10.1144/GSL.SP.1989.042.01.19

TIAN, Z.L. & WEI, C.J. 2014. Coexistence of garnet blueschist and eclogite in South Tianshan, NW China: dependence of *P–T* evolution and bulk-rock composition. *Journal of Metamorphic Geology*, **32**, 743–764.

TSUJIMORI, T. & ERNST, W.G. 2014. Lawsonite blueschists and lawsonite eclogites as proxies for paleo-subduction zone processes: A review. *Journal of Metamorphic Geology*, **32**, 437–454.

TSUJIMORI, T., SISSON, V.B., LIOU, J.G., HARLOW, G.E. & SORENSEN, S.S. 2006. Petrologic characterization of Guatemalan lawsonite eclogite: Eclogitization of subducted oceanic crust in a cold subduction zone.

In: HACKER, B.R., MCCLELLAND, W.C. & LIOU, J.G. (eds) *Ultrahigh-Pressure Metamorphism: Deep Continental Subduction*. Geological Society of America, Special Papers, **403**, 147–168.

WANG, Y.H., ZHANG, L.F., ZHANG, J.J. & WEI, C.J. 2017. The youngest eclogite in central Himalaya: P–T path, U–Pb zircon age and its tectonic implication. *Gondwana Research*, **41**, 188–206.

WEI, C.J. & POWELL, R. 2003. Phase relations in high-pressure metapelites in the system KFMASH (K_2O–FeO–MgO–Al_2O_3–SiO_2–H_2O) with application to natural rocks. *Contributions to Mineralogy and Petrology*, **145**, 301–315.

WEI, C.J. & POWELL, R. 2004. Calculated phase relations in high-pressure metapelites in the system NKFMASH (Na_2O–K_2O–FeO–MgO–Al_2O_3–SiO_2–H_2O). *Journal of Petrology*, **45**, 183–202.

WEI, C.J. & POWELL, R. 2006. Calculated phase relations in the system NCKFMASH (Na_2O–CaO–K_2O–FeO–MgO–Al_2O_3–SiO_2–H_2O) for high-pressure metapelites. *Journal of Petrology*, **47**, 385–408.

WEI, C.J. & TIAN, Z.L. 2015. Modelling of the phase relations in high-pressure and ultrahigh-pressure eclogites. *Island Arc*, **23**, 254–262.

WEI, C.J., POWELL, R. & ZHANG, L.F. 2003. Eclogites from the south Tianshan, NW China: petrologic characteristic and calculated mineral equilibria in the Na_2O–CaO–FeO–MgO–Al_2O_3–SiO_2–H_2O system. *Journal of Metamorphic Geology*, **21**, 163–179.

WEI, C.J., POWELL, R. & CLARKE, G.L. 2004. Calculated phase equilibria for low- and medium-pressure metapelites in the KFMASH and KMnFMASH systems. *Journal of Metamorphic Geology*, **22**, 495–508.

WEI, C.J., YANG, Y., SU, X.L., SONG, S.G. & ZHANG, L.F. 2009. Metamorphic evolution of low-T eclogite from the north Qilian orogen, NW China: Evidence from petrography and calculated phase equilibria in system NCKFMASHO. *Journal of Metamorphic Geology*, **27**, 55–70.

WEI, C.J., LI, Y.J., YU, Y. & ZHANG, J.S. 2010. Phase equilibria and metamorphic evolution of glaucophane-bearing UHP eclogites from the Western Dabieshan Terrane, Central China. *Journal of Metamorphic Geology*, **28**, 647–666.

WEI, C.J., QIAN, J.H. & TIAN, Z.L. 2013. Metamorphic evolution of medium-temperature ultra-high pressure (MT–UHP) eclogites from the South Dabie Orogen, Central China: an Insight from phase equilibria modeling. *Journal of Metamorphic Geology*, **31**, 755–774.

WEI, C.J., GUAN, X. & DONG, J. 2017. HT–UHT metamorphism of metabasites and the petrogenesis of TTGs. *Acta Petrologica Sinica*, **33**, 1381–1404.

WHITE, R.W., POWELL, R. & HOLLAND, T.J.B. 2001. Calculation of partial melting equilibria in the system Na_2O–CaO–K_2O–FeO–MgO–Al_2O_3–SiO_2–H_2O (NCKFMASH). *Journal of Metamorphic Geology*, **19**, 139–153.

WILL, T.M., POWELL, R. & HOLLAND, T.J.B. 1990*a*. A calculated petrogenetic grid for ultramafic rocks at low pressures in the system CaO–FeO–MgO–Al_2O_3–SiO_2–CO_2–H_2O. *Contributions to Mineralogy and Petrology*, **105**, 347–358.

WILL, T.M., POWELL, R., HOLLAND, T. & GUIRAUD, M. 1990*b*. Calculated greenschist facies mineral equilibria in the system CaO–FeO–MgO–Al_2O_3–SiO_2–CO_2–H_2O. *Contributions to Mineralogy and Petrology*, **104**, 353–368.

WILL, T.M., OKRUSCH, M., SCHMÄDICKE, E. & CHEN, G.L. 1998. Phase relations in the greenschist–blueschist–amphibolite–eclogite facies in the system Na_2O–CaO–FeO–MgO–Al_2O_3–SiO_2–H_2O (NCFMASH), with application to metamorphic rocks from Samos, Greece. *Contributions to Mineralogy and Petrology*, **132**, 85–102.

WINTHER, K.T. & NEWTON, R.C. 1991. Experimental melting of hydrous low-K tholeiite: evidence on the origin of Archaean cratons. *Bulletin of Geological Society of Denmark*, **39**, 213–228.

WYLLIE, P.J. & WOLF, M.B. 1993. Amphibole dehydration-melting: sorting out the solidus. *In*: PRITCHARD, H., ALABASTER, T., HARRIS, N. & NEARY, C. (eds) *Magmatic Processes and Plate Tectonics*. Geological Society, London, Special Publications, **76**, 405–416, https://doi.org/10.1144/GSL.SP.1993.076.01.20

XU, G.W., WILL, T.M. & POWELL, R. 1994. A calculated petrogenetic grid for the system K_2O–FeO–MgO–Al_2O_3–SiO_2–H_2O, with particular reference to contact-metamorphosed pelites. *Journal of Metamorphic Geology*, **12**, 99–119.

ZEN, E.A. 1966. *Construction of Pressure–Temperature Diagrams for Multicomponent Systems after the Method of Schreinemakers – A Geometric Approach*. United States Geological Survey Bulletin, **1225**.

ZHANG, C., HOLTZ, F., KOEPKE, J., WOLFF, P.E., MA, C. & BÉDARD, J.H. 2013. Constraints from experimental melting of amphibolite on the depth of formation of garnet-rich restites, and implications for models of Early Archean crustal growth. *Precambrian Research*, **231**, 206–217.

ZHANG, J.X., MENG, F.C. & WAN, Y.S. 2007. A cold Early Palaeozoic subduction zone in the North Qilian Mountains, NW China: petrological and U–Pb geochronological constraints. *Journal of Metamorphic Geology*, **25**, 285–304.